ELSEVIER

International Journal of Mass Spectrometry 207 (2001) 125–144

International Journal of Mass Spectrometry

Review

Electrospray mass spectrometry beyond analytical chemistry: studies of organometallic catalysis in the gas phase

Dietmar A. Plattner

Laboratorium für Organische Chemie, Eidgenössische Technische Hochschule (ETH) Zürich, CH-8092 Zürich, Switzerland

Received 19 December 2000; accepted 25 January 2001

Abstract

Electrospray tandem mass spectrometry, one of the most important techniques for the characterization of biological macromolecules, has become increasingly popular as an analytical tool in inorganic/organometallic chemistry. Going one step further, we have shown that the coupling of electrospray ionization to ion–molecule techniques in the gas phase can yield detailed information about elementary reaction steps of transition-metal compounds with fully intact coordination spheres. This method opens a door to the study of extremely reactive intermediates that have previously not been within reach of condensed-phase techniques. Moreover, working in the gas phase, information about the intrinsic reactivity of the complex itself is obtained, thus excluding solvent effects, aggregation phenomena etc. We have demonstrated the usefulness of this method for various important transition-metal mediated reactions such as C–H activation, oxidation, and olefin polymerization. Through the utilization of collision-induced dissociation (CID) threshold methodology, the quantitative measurement of thermochemical data for metal–ligand bond energies and elemental reaction steps is possible. In several instances, we have demonstrated that the CID threshold methodology can be applied to molecules with relatively many degrees of freedom, yielding experimental thermochemical data of high quality. Both the qualitative and quantitative reaction studies of organometallic intermediates will contribute to deepen our mechanistic understanding of important catalytic reactions. (Int J Mass Spectrom 207 (2001) 125–144) © 2001 Elsevier Science B.V.

Keywords: Electrospray ionization; Tandem mass spectrometry; Transition-metal catalysis, Ion–molecule chemistry; CID threshold measurements

1. Introduction

1.1. Why organometallic chemistry in the gas phase?

Gas-phase studies of metal ions and ionic transition-metal compounds and their reactivity have a long and distinguished history of over 25 years. The advancement of mass spectrometric ion–molecule techniques has made it possible to study single, elementary reaction steps mediated by transition-metal ions on both qualitative and quantitative levels [1]. Unfortunately, due to the limitations of "conventional" ionization techniques, the gas-phase chemistry of transition-metal compounds has for a long time been restricted to the study of compounds that would

* E-mail: plattner@org.chem.ethz.ch

PII S1387-3806(01)00371-2

hardly be considered as authentic catalysts by synthetic organometallic chemists. In other words, most studies had to confine themselves to singly and multiply charged "naked" ions and very simple organometallics of the type $[M(L)_n]^+$, with L some simple ligand, e.g. hydride, O, alkyl, CO, H_2O, etc. [2–6]. That such compounds bear hardly any resemblance to complexes present in condensed phases will, depending on the viewpoint, either be seen as virtue or vice. With some justification it has been pointed out that our knowledge of such highly unsaturated species is very limited so that research on such compounds is highly desirable [4]. On the other hand, our knowledge of key reaction mechanisms and especially the thermochemistry of transition-metal mediated reactions employing complexes with fully ligated spheres is also far from complete, which is why we started out to study the gas-phase chemistry of real catalysts.

When considering the possibilities of transferring real-world organometallics to the gas phase, one arrives at the conclusion that electrospray ionization (ES) should be the ideal technique, especially when the species of interest is already present in ionic form in solution. The motivation, advantages, and requirements for the experimental setup of gas-phase studies on organometallics can be summarized as follows.

Selection of species by mass to charge ratio: once in the gas phase, the species of interest can be singled out by mass spectrometric techniques, and their reactivity subsequently studied without perturbation by any of the other compounds present; thus, degradation in solution or during the ionization process does not pose problems.

MS/MS capabilities: in order to get structural information or to conduct reaction cascades, it is necessary to have at least two mass selection steps.

Study of intrinsic reactivity: the most important motivation for investigating gas-phase reactivities is to obtain information about the intrinsic reactivity of the molecule itself, which is not marred by solvent effects, aggregation phenomena etc.

Thermochemical parameters: ideally, we should not only be able to study the basic reactivity of organometallics, but also obtain thermochemical data of single reaction steps by quantitative collision-induced dissociation (CID) threshold measurements.

Stabilization of reactive intermediates: crucial intermediates in catalytic processes are often, by their very nature, extremely short lived; by transferring them to the gas-phase (or, alternatively, by transforming a suitable precursor in the gas phase) reactive intermediates are almost infinitely stable due to the high-vacuum conditions; the reactivity can then be probed by directed collision with reaction partners.

Direct transfer from solution to the gas phase: in most cases, the direct transfer of a well-characterized species from solution to the gas phase is desirable; for ionic organometallics, electrospray ionization has proven to be the best method due to its softness, i.e. even weakly bound ligands will remain intact.

1.2. Early mass spectrometric applications of electrospray

The softness of electrospray ionization has made this technique an indispensable tool for biochemical and biomedical research. Most applications have focused on the mass spectrometric characterization of biological macromolecules. Electrospray ionization has revolutionized the analysis of labile biopolymers, with applications ranging from the analysis of DNA, RNA, oligonucleotides, proteins as well as glycoproteins to carbohydrates, lipids, glycolipids, and lipopolysaccharides, often in combination with state-of-the-art separation techniques like liquid chromatography or capillary electrophoresis [7,8]. Beyond mere analytical applications, electrospray ionization mass spectrometry (ESMS) has proven to be a powerful tool for collision-induced dissociation and multiple stage tandem mass spectrometry (MS^n) analysis, and, beyond the elucidation of primary structures, even for the study of noncovalent macromolecular complexes [9].

Although a well-established technique [10], electrospray was not utilized for mass spectrometric applications before the late 1960s. Interested in determining molecular weight distributions of synthetic polymers, Dole and co-workers assembled an apparatus designed to stage the following scenario [11]: a dilute solution of the polymer analyte in a volatile

solvent is introduced through a small tube into an electrospray source chamber through which nitrogen as bath gas flows at atmospheric pressure. A potential difference of a few kilovolts between the tube and the chamber walls produces an intense electrostatic field at the tube exit and disperses the emerging solution into a fine spray of charged droplets. As the droplets lose solvent by evaporation their charge density increases until the Rayleigh limit is reached at which Coulomb forces overcome surface tension and the droplet breaks up into smaller droplets ("coulomb explosion"), which repeat that sequence. The rationale behind those experiments was that a succession of such coulomb explosions would finally lead to droplets so small that each would contain only one molecule of analyte. As the last of the solvent evaporates that residual molecule would retain some of the droplet charge, thereby becoming a free macro-ion. With polystyrene samples ranging in mass between 50 and 500 kDa in a benzene/acetone solvent mixture Dole et al. were able to demonstrate the formation of distinct macro-ions, which were concentrated in a supersonic jet and detected in a Faraday cage after small-molecular-weight ions had been repelled by suitable repeller voltages [12]. Even at this early stage, the authors mentioned the plan to build a time-of-flight mass spectrometer with an electrospray source. In subsequent studies, the method was further refined ("molecular beams of macro-ions") [13,14] and extended to the protein zein and polyvinyl pyrrolidone [15], but the limitations of the comparably low mass resolution in their setup could not be overcome due to experimental problems with the mass analysis and detection of macro-ions.

After those first attempts to develop analytical applications of electrospray, it took more than ten years for the first bona fide electrospray mass spectrometer to emerge [16]. Yamashita and Fenn published the first electrospray mass spectrometry experiment in a 1984 paper which was appropriately part of an issue of the *Journal of Physical Chemistry* dedicated to John Bennett Fenn [17]. They electrosprayed solvents into a bath gas to form a dispersion of ions that was expanded into vacuum in a small supersonic free jet. A portion of the jet was then passed through a skimmer into a vacuum chamber containing a quadrupole mass filter. With this setup, a variety of protonated solvent clusters as well as solvent–ion clusters (Na^+, Li^+) could be detected. Moreover, they extended the application to molecular beams of negatively charged ions [18]. Using an improved design of their electrospray ion source, Fenn and co-workers were also the first to couple high-performance liquid chromatography to a mass spectrometer by way of an electrospray interface [19].

1.3. ESMS and organometallic chemistry

The first applications of electrospray to the mass spectrometric characterization of biopolymers, including oligonucleotides and proteins, were also pioneered by J.B. Fenn and co-workers [20]. Strangely, despite the enormous impact of electrospray on the mass spectrometric characterization of biomolecules, applications to inorganic and organometallic chemistry had been lagging somewhat behind. Electrospray as a method of transferring pre-existing ions from solution to the gas phase should be ideally suited for inorganic and organometallic compounds which are in general not volatile and are thus difficult to ionize by conventional methods. Moreover, ionic main group and transition-metal solution species often bear weakly bound ligands, making a soft ionization technique mandatory. Thus, ESMS has become increasingly important as a primary characterization tool for "small-ion" solution chemistry. Electrospray mass spectra of tetraalkylammonium ions were already reported by Fenn and co-workers in the first of their electrospray publications [17,19]. The beginning of the utilization of electrospray ionization as a tool for the analysis of ionic transition-metal complexes is marked by a report on Ru^{II}-bipyridyl and 1,10-phentanthroline complexes by Chait and co-workers [21]. When spraying an acetonitrile solution at low ion-source collision energies, they observed a signal for the intact cation $[Ru^{II}(bpy)_3]^{2+}$ (bpy = bipyridyl) together with a series of lower intensity peaks resulting from the attachment of one to four acetonitrile molecules. At slightly higher energies, when the collisional activation is just sufficient for complete

desolvation, the mass spectrum was completely dominated by a single intense peak of $[Ru^{II}(bpy)_3]^{2+}$ ions. Upon further increase of collisional activation, the doubly charged ion dissociated, giving rise to signals for the fragments $[Ru^{II}(bpy)_2]^{2+}$ and $[Ru^{II}(bpy)]^{2+}$. As will be seen from the following paragraphs, it is very characteristic for the mass spectra of coordination complexes that fragmentation by collisional activation typically causes loss of a complete ligand rather than fragmentation of a ligand. This feature is particularly helpful for the identification and structural assignment of signals in the mass spectra.

Analytical applications of ESMS to transition-metal chemistry can be roughly divided into two groups: the mass spectrometric characterization of known and defined solution-phase species and the identification of crucial intermediates in transition-metal mediated reactions, whereby structural information can be obtained by CID, often in combination with other methods (electrochemistry, nuclear magnetic resonance spectroscopy). Both kinds of applications have already been extensively reviewed by Colton, D'Agostino, and Traeger in 1995 [22]. More recently, applications of ESMS in organometallic chemistry have been summarized with a focus on the ionization technique itself and its utilization in the characterization of transition-metal compounds [23]. The present account will therefore mainly deal with the gas-phase ion chemistry of transition metal complexes transferred to the gas phase by electrospray ionization.

2. Challenge of real-world catalysts

In principle, there are two different possibilities of studying highly reactive intermediates in organometallic catalysis within our experimental setup. In the first scenario, a not-too-low steady-state concentration of the species of interest is available in solution. After transfer to the gas phase, this complex can be singled out and studied further. If the compounds in solution do not degrade within a few minutes, it will also be possible to conduct CID threshold studies that way. In the second scenario, a suitable stable precursor complex is present in solution. After electrospray, the reactive species is generated by collisional activation, say, by loss of one or several ligands. In this case, lability in solution is ruled out completely.

2.1. Experimental setup and modes of operation

An experimental setup that meets the demands posed in the introductory remarks is the electrospray ionization tandem mass spectrometer. The apparatus used in our experiments is shown schematically in Fig. 1. In a typical experiment, a 10^{-4} to 10^{-5} M solution of the transition-metal compound in a polar organic solvent (preferentially acetonitrile or dichloromethane) is pressed through a capillary at a flow rate of 7–15 μl/min and electrosprayed at a potential of 4–5 kV using N_2 as sheath gas. The ions are then passed through a heated capillary (typically at 150–200 °C) where they are declustered and the remaining solvent molecules evaporate. The extent of desolvation and collisional activation can further be controlled by a tube lens potential in the electrospray source which typically ranges from 35 (mild conditions) to 75 V (hard conditions). The first octopole (O1) acts as an ion guide to separate the ions from neutral molecules, which are pumped off by a turbopump located underneath the octopole. O1 is fitted with an open cylindrical sheath around the rods into which, depending on the setup, a collision gas can be bled for thermalization or reaction at pressures up to 100 mTorr. The ions then enter the actual mass spectrometer, which is at 10^{-6} Torr and 70 °C manifold temperature during operation [Fig. 1(b)]. The configuration is quadrupole/octopole/quadrupole (Q1/O2/Q2), with the two quadrupoles as mass selection stages and the second octopole operating as a CID cell. Spectra are recorded in three different modes. In the normal ESMS mode, only one quadrupole is operated (either Q1 or Q2), and a mass spectrum of the electrosprayed ions is recorded. This mode serves primarily to characterize the ions produced by a given set of conditions. In the daughter-ion mode, Q1 is used to mass-select ions of a single mass-to-charge ratio from among all of the ions produced in O1, which are then collided or reacted with a target gas in O2, and finally mass analyzed by Q2. This mode is used to obtain structural information (by analysis of the fragments) or

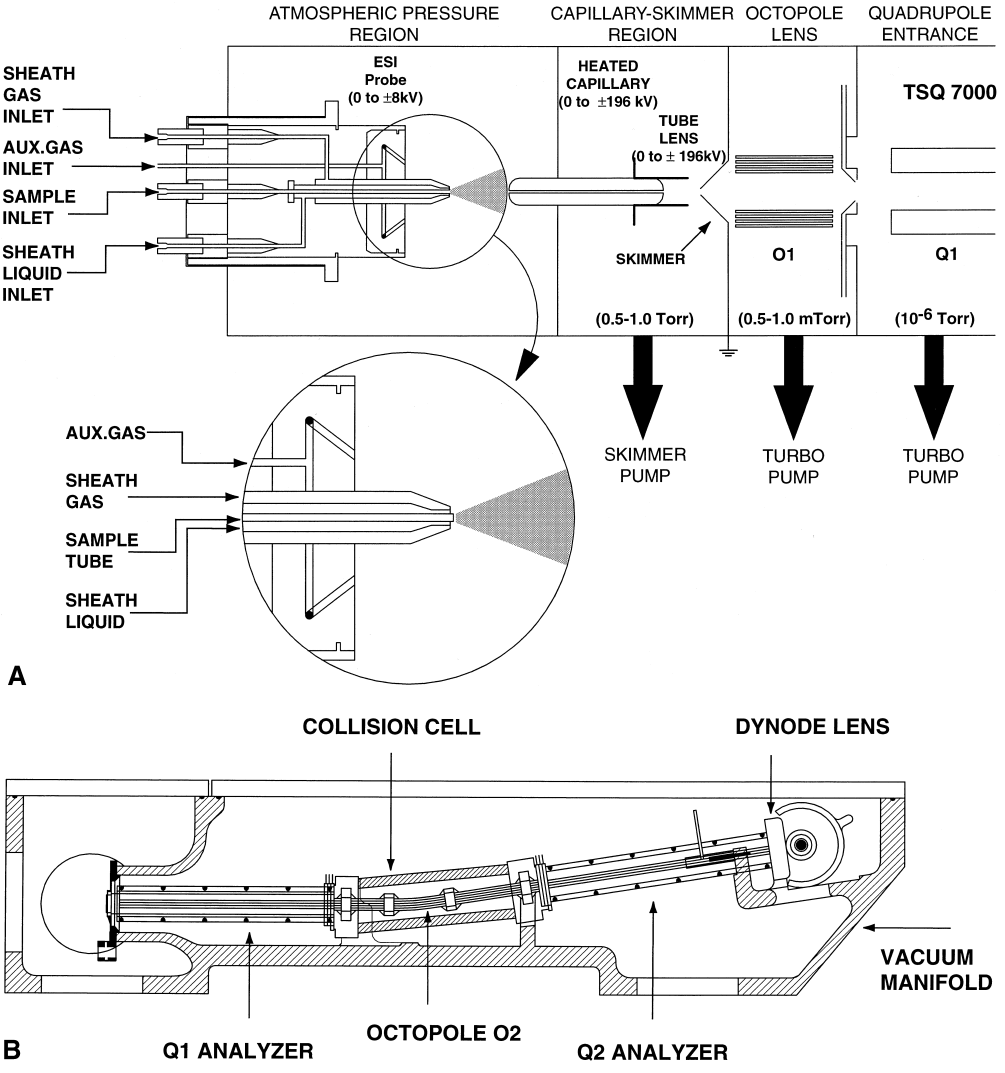

Fig. 1. Schematic representations of (a) the electrospray source and (b) the mass analyzer assembly.

the specific reactivity of a species of a given mass. The third mode of operation, the RFD mode (radio frequency daughter mode), is used to record CID thresholds for quantitative thermochemical measurements (see the following). Ions produced in O1 are mass selected, with Q1 acting as a high-pass filter. The selected ions are then collided with a target gas in O2, and mass analyzed in Q2. In the RFD mode, the reaction of ions in a particular mass range are isolated by setting the mass cutoffs above and below the desired range and then substracting the latter from the former spectra.

2.2. Model studies

One of the earliest examples of nonanalytical applications of electrospray ionization was the coupling of ES to ion–molecule techniques in the gas phase by Posey and co-workers [24]. They electrosprayed methanolic solutions of $Fe(bpy)_3(ClO_4)_2$ to produce molecular beams of complexes of divalent transition metal ions [24]. The residual electrospray solvent was removed from the gas-phase ions by collisional activation, and clusters were formed by the association of solvent

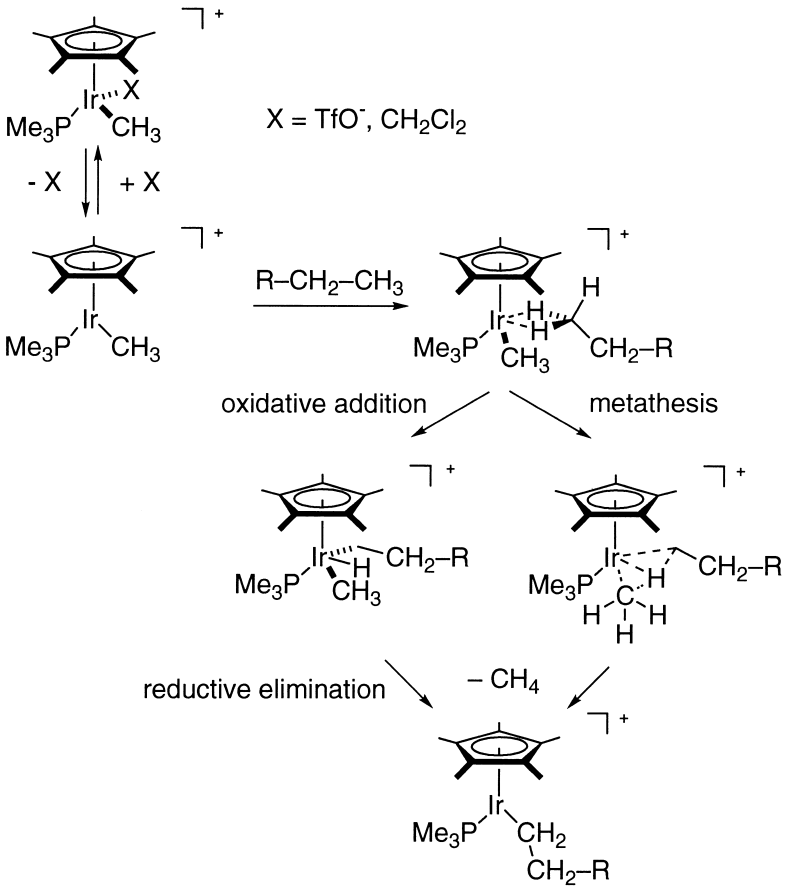

Scheme 1. Mechanism for the C–H activation by cationic iridium(III) complexes proposed by Bergman and co-workers [27].

molecules from the purge in an expansion as the ions passed through the first and second stages of differential pumping in the ES source. By this method, clusters of $[Fe(bpy)_3]^{2+}$ with a variety of solvents (acetone, acetonitrile, *N*,*N*-dimethylformamide, alcohols, etc.) were prepared by introducing the solvent of choice to the nitrogen purge [24a]. Metal-to-ligand charge transfer in the gas-phase ions and clusters was then probed by laser photofragmentation mass spectrometry. Excitation in clusters triggers evaporation of neutral solvent molecules, e.g. methanol, as the system relaxes. The wavelength-dependent photodissociation yield was measured between 530 and 600 nm for mass-selected $[Fe(bpy)_3 \cdot (CH_3OH)_n]^{2+}$ clusters ($n = 2—6$). The resulting photodissociation action spectra reflected the onset of the metal-to-ligand charge transfer absorption band as a function of cluster size [24b]. The solvent dependence of the charge transfer was further studied for terpyridyl iron complexes $[Fe(terpy)_2]^{2+}$ in clusters with one or four molecules of polar, organic solvents (acetone, acetonitrile, dimethylsulfoxide, *N*,*N*-dimethylformamide, etc.) [24c].

2.3. C–H activation by cationic iridium(III) complexes

The search for a homogeneous transition-metal catalyst capable of selective insertion into nonactivated C–H bonds of alkanes and arenes is generally acknowledged to be one of the most important tasks in chemistry [25]. In the early 1980s, rhodium and iridium Cp* complexes with the metal in the oxidation states +1 and +3, respectively, have been found

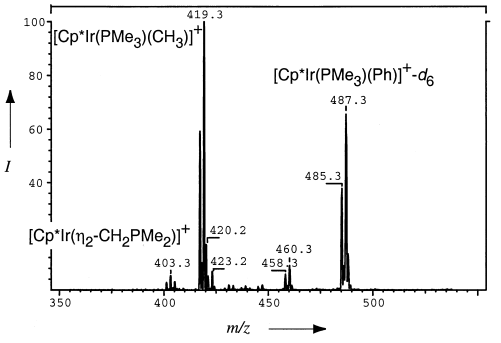

Fig. 2. Electrospray mass spectrum showing a mixture of $[Cp^*Ir(PMe_3)(CH_3)]^+$ (m/z = 417,419) and $[Cp^*Ir(PMe_3)(Ph)]^+$-d_6 (m/z = 485,487), prepared by reaction of $[Cp^*Ir(PMe_3)(CH_3)]^+$ and $[Cp^*Ir(\eta^2\text{-}CH_2PMe_2)]^+$ with benzene-d_6.

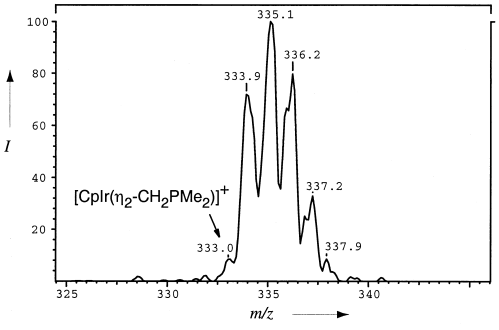

Fig. 3. Expansion of the CID spectrum of $[CpIr(PMe_3)(Ph)]^+$-d_6, showing the formation of various deuterated three-ring species $[CpIr(\eta^2\text{-}CH_2PMe_2)]^+$-$d_x$ (x = 0–6).

to be the most promising candidates to achieve this task [26]. The search for a catalyst active under milder conditions led Bergman to the introduction of cationic iridium(III) complexes (Scheme 1) [27]. These complexes perform C–H activation without prior photochemical or thermal activation, and are therefore particularly interesting as model systems ultimately leading to catalytic cycles. The actual reactive species was presumed to be the 16-electron complex $[Cp^*Ir(PMe_3)(CH_3)]^+$, which would be formed from the 18-electron precursor by dissociation of a weakly bound ligand in solution.

Two mechanisms have been suggested to account for the observed reaction products [27]: an oxidative addition/reductive elimination sequence of reactions and a concerted σ-bond metathesis reaction. This concerted mechanism comes into consideration for the iridium(III) complex because it might be unfavorable for the strongly electron-deficient 16-electron

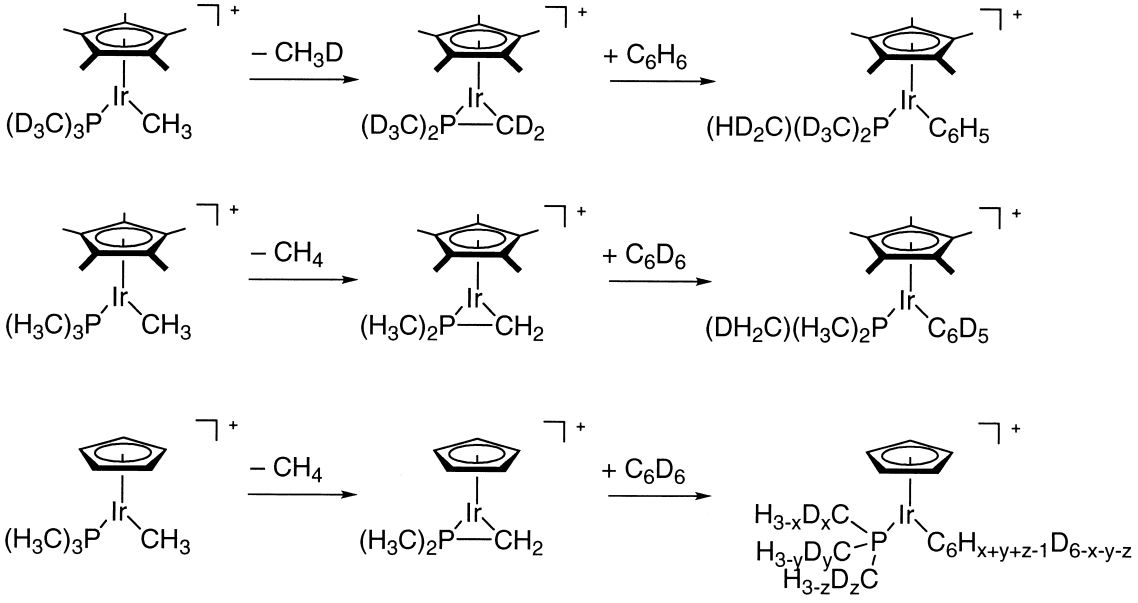

Scheme 2. Deuterium-labeling experiments indicating the presence of a three-membered ring intermediate.

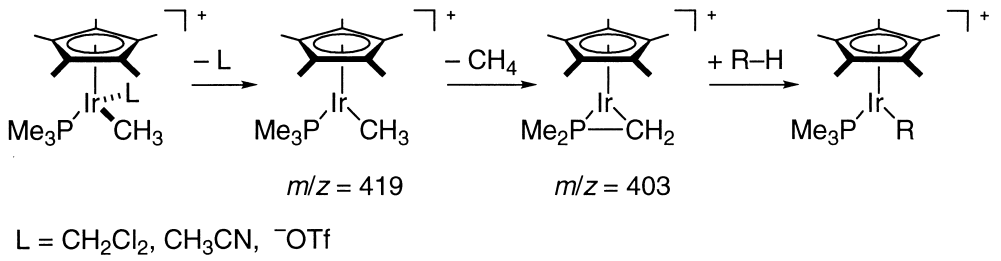

Scheme 3. The "dissociative-associative" mechanism of C–H activation by cationic iridium(III) complexes.

Ir(III)-complex to engage in an oxidative addition step resulting in a formally Ir(V) species. According to hybrid Hartree-Fock/density functional calculations by Hall and co-workers [28], the oxidative addition/reductive elimination route is more likely than the concerted mechanism.

In order to obtain insight into the detailed mechanism of C–H activation we studied the gas-phase reactivity of both $[Cp^*Ir(PMe_3)(CH_3)]^+$, the proposed reactive species in the Bergman system, and the Cp-analogue $[CpIr(PMe_3)(CH_3)]^+$ [29,30]. They were generated by electrospray of acetonitrile solutions of $[Cp^*Ir(PMe_3)(CH_3)(CH_3CN)]^+$ ClO_4^- and the corresponding salt of the Cp analogue. Electrospray under mild desolvation conditions produced the unfragmented cation, whereas a slight increase in the tube lens potential, i.e. higher collisional activation in the desolvation region of the electrospray source, led to almost complete loss of the acetonitrile ligand, leaving predominantly the bare, unsolvated 16-electron complex cation $[Cp^{(*)}Ir(PMe_3)(CH_3)]^+$. Much to our surprise, neither $[Cp^*Ir(PMe_3)(CH_3)]^+$ nor the more electron-deficient $[CpIr(PMe_3)(CH_3)]^+$ showed any appreciable reactivity toward hydrocarbons in the gas phase. Under typical reaction conditions, i.e. benzene at ~10 mTorr as target gas at collision energies ranging between 3 and 20 eV, the signal for the 16-electron cation remains unchanged.

At this point, another peak growing in the spectrum when raising the tube lens potential caught our attention. Higher collisional activation not only causes complete dissociation of acetonitrile, but also induces a chemical reaction leading to a loss of 16 mass units. Application of still higher tube lens potentials in the source yields predominantly an iridium complex with $m/z = 403$, a species which adds readily to benzene in the collision cell, as can be seen from Fig. 2. Based on deuterium-labeling experiments (Scheme 2), the structure of the signal at $m/z = 403$ was assigned as $[Cp^*Ir(\eta^2\text{-}CH_2PMe_2)]^+$, the product of cyclometalation with one of the phosphine methyl groups and concomitant loss of methane. A very elegant proof for the cyclometalation intermediate is provided by the reactivity of the Cp complex $[CpIr(PMe_3)(CH_3)]^+$. In this case, not only one deuterium is incorporated in the ligand, but six deuterium atoms of the incoming benzene are completely scrambled over the phosphine (Fig. 3). There are two reasons for this behavior: the reaction of the three-membered ring intermediate with the hydrocarbon is reversible and in the case of the Cp complex, the attractive forces between $[CpIr(\eta^2\text{-}CH_2PMe_2)]^+$ and benzene are large enough so that dissociation is not complete in the reverse reaction, and the addition/elimination sequence can occur multiple times with the same reaction partners. The three-membered ring intermediate does not only react with benzene, but also adds to less reactive hydrocarbons as methane, pentane, or cyclohexane [30]. However, their C–H activation products show a different reactivity pattern. Thus, the product of the addition to pentane, $[Cp^*Ir(PMe_3)(C_5H_{11})]^+$, undergoes β-hydride elimination when collided with a target gas to yield $[CpIr(PMe_3)(H)]^+$. With alkyl ligands at Ir^{III}, the reverse cyclometalation is obviously not a feasible pathway in competition with the facile elimination of pentene.

Our gas-phase investigation of the reactivity of cationic iridium(III) complexes toward hydrocarbons

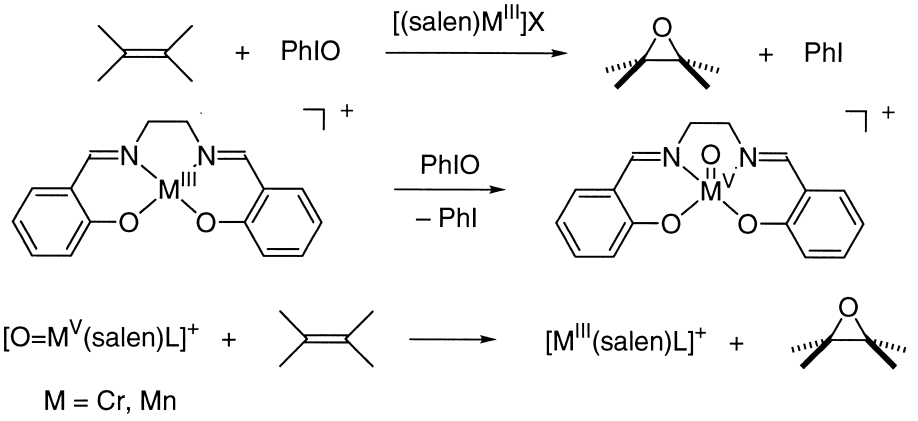

Scheme 4. The mechanism of alkene epoxidation catalyzed by metal–salen complexes.

revealed a new, previously unreported mechanism for the observed σ-bond metathesis reactions (the "dissociative-associative mechanism," Scheme 3). In contrast to a two-step mechanism involving intermolecular oxidative addition of the 16-electron complex to the C–H bond of a hydrocarbon producing an Ir(V) intermediate, followed by reductive elimination of methane, or a concerted σ-bond metathesis reaction similar to that seen in early transition metals, the electrospray mass spectra show a different mechanism to be operative, involving initial elimination of methane in an intramolecular reaction, followed by addition to the hydrocarbon.

The question may arise how this knowledge of the intrinsic reactivity of cationic iridium(III) complexes with regard to C–H activation could be utilized for the design of more efficient catalysts. Fortunately, we did not have to wait too long before an answer to this question was given. It was less than one year after publication of our gas-phase results [29,30] that Luecke and Bergman reported the solution-phase reactivity of $Cp^*Ir(\eta^2\text{-}CH_2PMe_2)(OTf)$ (TfO^- = trifluoromethanesulfonate), a catalyst which had been designed according to the reactivity scheme found in our electrospray work [31]. The rate of disappearance of the precursor complex $Cp^*Ir(\eta^2\text{-}CH_2PMe_2)(Cl)$, from which $Cp^*Ir(\eta^2\text{-}CH_2PMe_2)(OTf)$ is formed by adding AgOTf, in neat benzene is extremely rapid ($t_{1/2}$ = 5 min at 25 °C), much faster than the analogous reaction of $Cp^*Ir(PMe_3)(CH_3)(OTf)$ ($t_{1/2}$ = 24 h at 25 °C). The iridaphosphacyclopropane complex formed from $Cp^*Ir(PMe_3)(CH_3)(OTf)$ is much superior in C–H activation as compared to the 16-electron complex $[Cp^*Ir(PMe_3)(CH_3)]OTf$. This solution-phase reactivity resembles exactly the order of reactivity we found in the gas-phase experiments. This was a perfect demonstration how useful knowledge about reaction mechanisms obtained from ion–molecule reactions in the gas phase can be for the design of novel, superior solution-phase catalysts.

2.4. High-valent oxomanganese complexes

The mechanistic scheme for oxygen transfer to organic substrates by manganese–salen and porphyrin complexes is based on the isolation and characterization of the oxochromium(V) species by Kochi and co-workers (Scheme 4) [32a,c]. The oxochromium–salen complex was prepared by oxidation of the chromium(III) precursor with PhIO, isolated, and shown to be capable of epoxidizing alkenes under stoichiometric and catalytic conditions [32b]. This result was in accordance with the properties and reactivity of an analogous oxoporphinatochromium(V) complex studied earlier by Groves and Kruper [33]. The metal-oxo species in these reactions are acting as a staging post for oxygen transfer, which is why the mechanism was termed "oxygen-rebound."

The chromium complexes were useful for mechanistic studies, but their utility as epoxidation catalysts is limited to electron-rich olefins. Switching to manganese, Kochi and co-workers established a much more versatile salen-based oxidation catalyst [32d,e]. The introduction of chiral manganese–salen catalysts by Jacobsen and co-workers achieved a breakthrough in the field of enantioselective epoxidation [34]. A similar, but by and large, less effective system was developed by Katsuki and co-workers at around the same time [35]. The Jacobsen-Katsuki reaction is now established as one of the most useful and widely applicable methods for the epoxidation of unfunctionalized olefins. However, mechanistic studies on these systems as well as the chemically similiar manganese– and iron–porhyrin complexes have so far been hampered by the fact that the catalytically active oxometal species appear only as fleeting putative intermediates.

In view of the fact that oxygen transfers are so common and important in nature and chemical synthesis it may seem surprising that our knowledge of the detailed mechanisms of these reactions leaves much to be desired. Two factors are mainly responsible for the lack of mechanistic insights: oxygen transfer to the transition metal by dioxygen or some single oxygen atom donor can yield several different species with quite diverse reactivities, and the transient nature of the catalytically active species precludes characterization. Both problems can easily be overcome by transfer of the metal–oxo complexes to the gas phase and subsequent study of ion–molecule reactions. Electrospray mass spectra of $[(salen)Mn^{III}]^+$ ClO_4^- solutions with and without addition of a suitable oxygen-transfer reagent are shown in Fig. 4 [36,37]. The oxidized species which were detected by ESMS are listed in Scheme 5; the parent oxo complex $[O{=}Mn^{V}(salen)]^+$ (m/z = 337) and the μ-oxo bridged dimer with two capping PhIO ligands $[PhIO(salen)Mn{-}O{-}Mn(salen)OIPh]^{2+}$ (m/z = 549) give rise to the most prominent peaks.

The detection of $[PhIO(salen)Mn{-}O{-}Mn(salen)OIPh]^{2+}$ in our electrospray experiments was the first direct evidence for the conproportionation of Mn^{III} and Mn^{V}–oxo species as the mechanism for parking

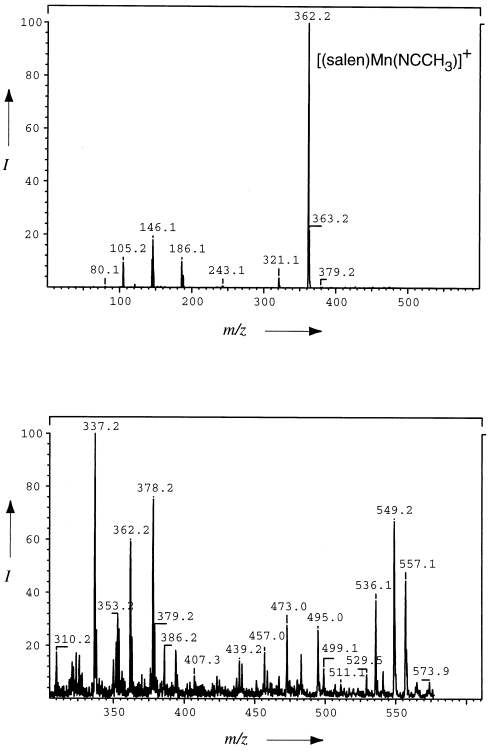

Fig. 4. (Top) Electrospray mass spectrum of an acetonitrile solution of $[(salen)Mn(NCCH_3)]^+$ (m/z = 362), showing the unfragmented complex as well as the ion produced by solvent ligand loss (m/z = 321). (Bottom) Electrospray mass spectrum of an authentic epoxidation reagent mixture obtained by adding PhIO to an acetonitrile solution of $[(salen)Mn(NCCH_3)]^+$.

the catalytically active complex in a more persistent form. The reverse process, the disproportionation of the μ-oxo bridged dinuclear complex, leads to the release of the active $[O{=}Mn^{V}(salen)]^+$. This reaction can be induced by a collision experiment in the gas phase, thus providing a structural proof for the parent dication as well as for the reactive oxomanganese(V) cation. The daughter-ion experiment with $[PhIO(salen)Mn{-}O{-}Mn(salen)OIPh]^{2+}$ (m/z = 549) led to the expected disproportionation products $[PhIO(salen)Mn^{III}]^+$ and $[PhIO(salen)Mn^{V}{=}O]^+$. The two primary daughter ions formed by collisional activation immediately fragment further, giving rise to a quite complex product pattern.

The coordination chemistry of iodosobenzene and the mechanism of oxygen transfer to the metal center

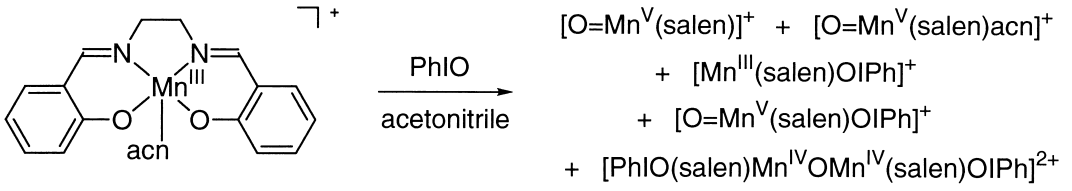

Scheme 5. Species detected by ESMS upon oxidation of $[(salen)Mn^{III}]^+$.

were also examined by collision-induced dissociation [37]. The daughter-ion spectrum of $[PhIO(salen)Mn^{III}]^+$ displays the following reactivity: the only product peak observed is the $O{=}Mn^{V}$(salen) complex due to exclusive fragmentation of the O–I bond. CID on the oxo-complex $[PhIO(salen)Mn^{V}{=}O]^+$, however, leads mainly to loss of iodosobenzene (→$[(salen)Mn^{V}{=}O]^+$. When compared to the daughter-ion spectrum of $[PhIO(salen)Mn^{III}]^+$, it is obvious that the formation of $[O(salen)Mn^{V}O]^+$ (we regard the rearrangement to a peroxomanganese(V) complex to be highly improbable) is not very favorable.

CID experiments revealed the nature and structure of the oxidized species present in manganese–salen catalyzed epoxidation reactions. What remained to be demonstrated was the oxomanganese(V) species' capability of transferring oxygen to organic substrates. This was proven by collision experiments with substrates that are also oxidized by the catalytic system in solution, namely electron-rich olefins and sulfides. When $[O{=}Mn^{V}(salen)]^+$ is mass selected in the first quadrupole and then collided with an inert gas (1 mTorr of argon) in the second octopole at collision energies up to 20 eV, no fragmentation can be induced. This is in agreement with the structure of the oxo complex, because it is highly unlikely that all four ligand–metal bonds or the strong manganese-oxo bond would fragment. This feature enabled us to probe the reactivity of the oxomanganese(V) species. The oxidized substrates bearing no charge cannot be detected in our setup, but collision with 2,3-dihydrofuran or dimethylsulfide leads to the formation of $[(salen)Mn^{III}]^+$ (m/z = 321, Scheme 6). Since we had shown that the detection of a species at m/z = 321 complex cannot be the result of fragmentation, it was established that the appearance of this peak is due to oxygen transfer from the oxomanganese(V) complex to the substrate.

The diverse coordination chemistry of manganese(III) and oxomanganese(V) salen in the gas phase was also studied using electrospray ionization and subsequent application of tandem mass spectrometric techniques [38]. The formation of five- versus six-coordinate manganese(III) species was probed by ion–molecule reactions with neutral ligands, e.g. acetonitrile, pyridine, alcohols, etc. The reactivity of the highly elusive oxomanganese(V)–salen complexes, generated by fragmentation of dinuclear μ-oxomanganese(IV) complexes (see previous discussion), and their coordination chemistry was studied in the same way. The effects of axial ligation on the reactivity of the oxo complexes were found to be quite drastic. The epoxidation of olefins by oxomanganese(V)–salen was studied intramolecularly by tethering the substrate to the metal center. No indication for pre-

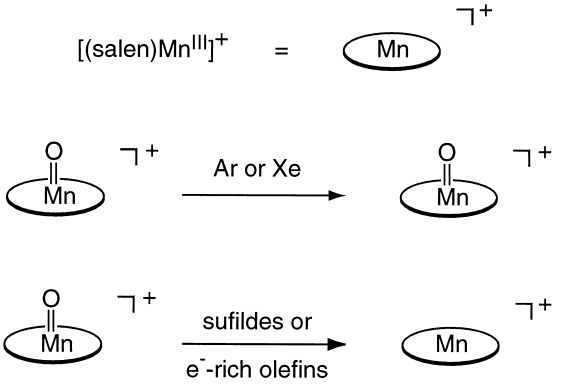

Scheme 6. Reactions of $[(salen)Mn{=}O]^+$ in the gas phase. While no fragmentation occurs upon CID with inert gases, the manganese(III) complex is regenerated in the presence of oxygen acceptors.

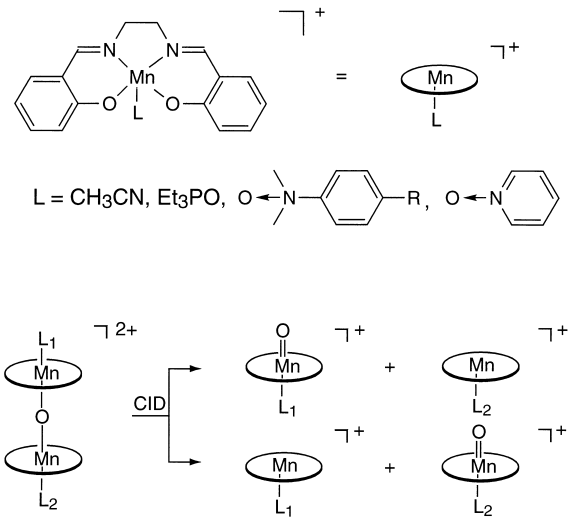

Scheme 7. Possible fragmentation products upon CID of μ-oxo-manganese(IV)–salen complexes bearing two different terminal ligands on each side.

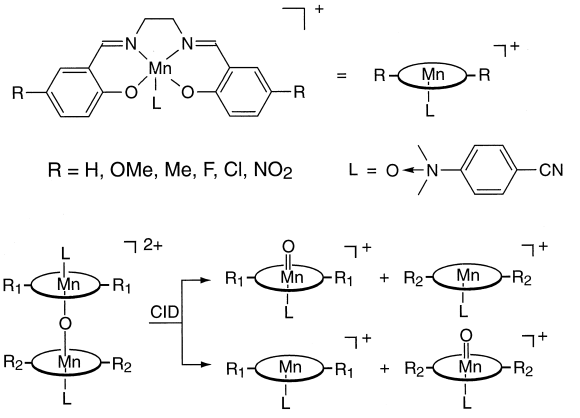

Scheme 8. Possible fragmentation products upon CID of μ-oxo-manganese(IV)–salen complexes with salen ligands differently substituted in the 5 and 5′ positions.

coordination of the substrate as prerequisite for oxidation was found.

By comparing the coordination chemistry of manganese(III) and oxomanganese(V) complexes, we arrived at the conclusion that the influence of axial ligation on the catalytically active species had so far been seriously underestimated. For condensed-phase reactions, it had been shown that adding donor ligands to the reaction mixture can alter the oxidation kinetics [32b,e]. The question arises whether or not the donor ligands directly affect the reactivity of the oxygen-transferring species. The presence of the μ-oxomanganese(IV) complexes led us to devise the following methodology to assess ligand effects on the reactivity of the Mn=O species: when a dinuclear μ-oxo complex with different axial ligands on each side is fragmented, the ratio of the resulting two oxomanganese(V) complexes (and, accordingly, the corresponding (salen)Mn^{III} fragments) will reflect their kinetic stability (Scheme 7) [39]. It is assumed that the reverse barrier for both reaction channels is roughly equal, i.e. entropic factors cancel, and that the energy distribution of the reactant ions can be approximated by a Boltzmann distribution. This implies that the observed difference in kinetic stability will reflect the difference in thermodynamic stability as well [40]. Thus, it becomes possible to establish an ordering of the relative stabilities of oxomanganese(V)–salen complexes depending on the influence of the axial ligand. For various amine *N*-oxides and triethylphosphine oxide it was shown that the axial ligand decreases the stability and thus enhances the reactivity of the Mn=O moiety. By competition experiments between those ligands their relative efficiency as promoters in the epoxidation could be established.

Addition of donor ligands is not the only way to tune the epoxidation reactivity of salen complexes. It was early recognized by Kochi that (salen)Mn complexes with electron-donating substituents such as the 5,5′-dimethoxy derivative effect only poor yields of epoxide, whereas the catalyst with 5,5′-dinitro substituents gave the best product yields. Using the same methodology as for the axial ligands (Scheme 8), we chose the following salen derivatives for the competition experiments: 5,5′-dinitro; 5,5′-difluoro; 5,5′-dichloro; 5,5′-dimethyl; 5,5′-dimethoxy; and the unsubstituted salen itself. We found the destabilizing effect on the oxomanganese(V) complex to be in the following order: $NO_2 > Cl \simeq H > F > CH_3 >$ OMe (the effect of NO_2 could not be quantified exactly due to rapid decomposition of the sample solutions). The product yields in the fragmentation experiments reflect the trend in stability of the oxo-

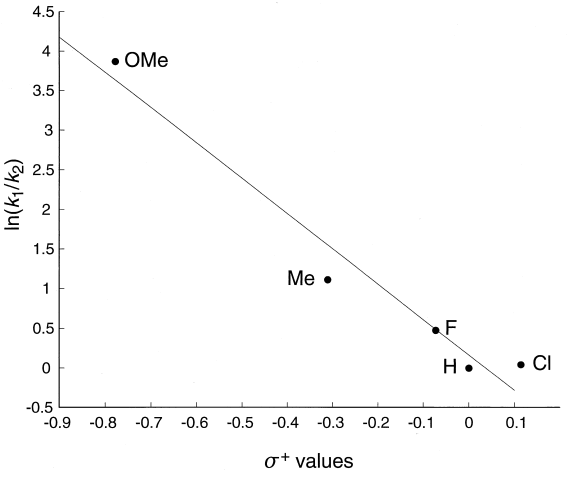

Fig. 5. Correlation of the branching ratios of "mixed" μ-oxomanganese(IV)–salen complexes and σ^+ values of the 5,5′ substituents.

manganese(V) ions that one would conceive intuitively considering the electronic properties of the substituted salen ligands. The Mn=O moiety in these high-valent complexes is stabilized by electron donating and destabilized by electron-withdrawing substitutents. This result can easily be rationalized by the electron deficiency imposed on the manganese center upon oxidation to Mn^{V}=O. The differences in stability derived from gas-phase experiments are quite pronounced. The ordering of the substituent effects suggests an underlying linear–free-energy relationship. When plotting $\ln(k_1/k_2)$ versus Hammett parameters found in the literature, the best correlation was obtained with the σ^+ values given by Brown and Okamoto (Fig. 5) [41]. The good correlation with the σ^+ values in our experiments can be rationalized by the analogy between a developing carbocation and the increase in oxidation state of the manganese center in the course of the fragmentation.

By using electrospray to transfer authentic reaction mixtures to the gas phase, we are able to study the reactivity and properties of species that could so far not even be characterized in solution due to their inherent reactivity/instability. CID experiments help us further to establish a relative order of reactivity of the previously elusive high-valent oxomanganese complexes.

2.5. Ziegler-Natta-like olefin oligomerization by alkylzirconocene cations

The Ziegler-Natta polymerization of olefins is a technical process of utmost importance for the synthesis of high-molecular-weight polymers [42]. The technical process is based on the activation of a suitable zirconocene precursor, typically Cp_2ZrMe_2 or Cp_2ZrCl_2, by a strong Lewis acid as co-catalyst (e.g. methylaluminoxane MAO, the product of a partial hydrolysis of $AlMe_3$). The co-catalyst has a twofold function in the technical process: it assures partial or complete alkylation if the precursor is a zirconocene dihalide and due to its strong Lewis acidity, MAO removes one of the methyl groups of dimethylzirconocene, thus forming an ion pair $[Cp_2ZrCH_3]^+$ CH_3–MAO^- where the cation is not free, but stabilized by $Al_2O\rightarrow Zr$ or $AlCH_3\rightarrow Zr$ contacts.

Mechanistic studies on Ziegler-Natta-like polymerization soon concentrated on the role of cationic alkylzirconocene species in the catalysis. In the mid 1980s, Jordan and co-workers were the first to isolate and characterize the alkylzirconocene cation $[Cp_2Zr(CH_3)(THF)]^+$ $[BPh_4]^-$ [43]. Due to the predissociation of THF being the rate-limiting step, the ethylene polymerization activity of this methylzirconocene salt is relatively low. In solvents acting as donor ligands (THF, acetonitrile) its polymerization activity is shut down completely. These results supported the original proposal (the so-called Long-Breslow-Newburg mechanism) that a cationic alkylzirconocene is the active species in Ziegler-Natta polymerization. A breakthrough was achieved by the introduction of perfluorinated tetraphenylborate as a counterion [44]. Those salts were the first well-defined zirconocene complexes that could polymerize propene and higher olefins without the addition of an activator.

There had been previous mass spectrometric studies of isolated metallocene ions in the gas phase, most notably by Eyler, Richardson and co-worker [45]. They prepared $[Cp_2ZrCH_3]^+$ by electron impact on dimethylzirconocene, but the reaction with olefins invariably led to production of allylic complexes. The allylic complexes formed by H_2 and CH_4 loss are

catalytically inactive in further olefin insertion steps. Ziegler-Natta-like oligomerization of α-olefins could never be observed in those ion cyclotron resonance (ICR) experiments. Richardson and Eyler attributed the difference between their results and the condensed-phase reactivity to incomplete thermalization of the intermediate ions in the very low-pressure environment of an ICR spectrometer cell. Since the second octopole in our experimental setup is operated at much higher pressures when used as a reaction cell, the conditions to carry off the reaction energy are much more favorable.

We prepared stable solutions of the tetrakis(pentafluorophenyl)borate salt of the methylzirconocene cation $[Cp_2ZrCH_3]^+$ by treatment of an acetonitrile solution of $Cp_2Zr(CH_3)_2$ with dimethylanilinium tetrakis(pentafluorophenyl)borate. The solution was then electrosprayed with a "high" pressure of thermalization gas (10 mTorr argon) in the first octopole region, thus generating a dominant peak corresponding to $[Cp_2Zr(CH_3)(CH_3CN)]^+$ [46]. More severe desolvation conditions, i.e. higher tube lens potentials, produce predominantly $[Cp_2Zr(CH_3)]^+$, which was thermalized to 70 °C and subsequently reacted in the second octopole with 1-butene. The products observed reflected the reactivity which had already been seen in the ICR experiments: not the insertion product $[Cp_2Zr(C_5H_{11})]^+$ ($m/z = 291$) was formed, but exclusively the allylic complex $[Cp_2Zr(C_5H_9)]^+$. Raising the pressure of the reactant even higher solved the problem. Use of 1-butene in the first ocotopole for reaction and thermalization produced the insertion product $[Cp_2Zr(C_5H_{11})]^+$.

Mass selection of $[Cp_2Zr(C_5H_{11})]^+$ in the first quadrupole and collision with 1-butene at 10 mTorr and near-zero collision energy in the second octopole produced the daughter-ion mass spectrum shown in Fig. 6. Although the reaction in the first octopole led to a quite complex product mixture, the reaction of mass-selected $[Cp_2Zr(C_5H_{11})]^+$ in the second octopole was remarkably clean, and addition of further units of the olefin occurred up to $[Cp_2Zr(CH_2CHEt)_4CH_3]^+$. Experiments with 1-pentene gave similar results. With ethylene or propylene, however, H_2 loss was more difficult to suppress.

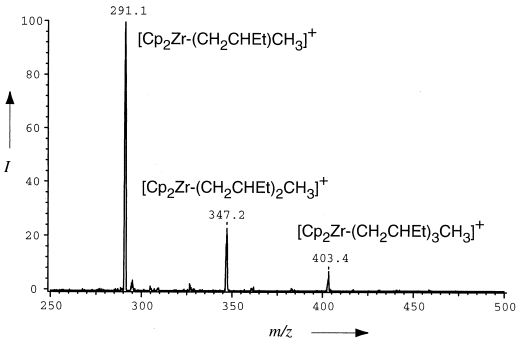

Fig. 6. Daughter-ion spectrum of the products from the gas-phase reaction of $[Cp_2Zr(C_5H_{11})]^+$ ($m/z = 291$) and 1-butene. The peaks at $m/z = 347$ and 403 correspond to the addition of one and two olefin molecules.

The most notable difference between our gas-phase results and the analogous reaction in solution is the large rate acceleration. A kinetic study of the Cp_2ZrCl_2/MAO system in solution-phase olefin polymerization found $k_p = 168 - 1670\ M^{-1}\ s^{-1}$ at 70 °C [47]. To estimate the second-order rate constant for the addition of 1-butene to $[Cp_2ZrR]^+$, we modeled the ion mobility in the octopole collision cell using a Monte Carlo simulation assuming a Langevin cross section for the collision rate, which gave, depending on the conditions, up to 100000 collisions of the incident ions with target gas molecules before exit. Comparing the measured product yield with the number of collisions gave a reaction probability per collision of about 10^{-3}, which corresponds to a second-order rate constant of $k \sim 10^8 - 10^9\ M^{-1}\ s^{-1}$ at 70 °C. The dramatic difference to the solution-phase kinetics is due to the following reasons: lacking a counterion or any charge donation by coordinating solvent molecules, and furthermore lacking any pre-equilibria to form the active species, the isolated cations should be intrinsically more reactive and the electrostatic interaction, either ion dipole or ion induced-dipole, which is screened out in solution, effectively lowers the activation barrier of a bimolecular ion–molecule reaction by a few kcal/mol relative to the same reaction in solution.

3. Quantitative CID threshold measurements

3.1. General remarks

We have already pointed out that one of the advantages of carrying out organometallic reactions in the gas phase is the possibility to obtain thermochemical data for single reaction steps. This is in strong contrast to measurements in solution, e.g. calorimetry, where reaction enthalpies of a single transformation can in principle be measured, but will always be affected by side reactions, solvent effects (if only caused by reorganization of the solvent sphere), etc. The actual problem with transition metal chemistry in condensed phases lies in its complexity. One can never be sure about the nature of the actual reactive species, which may be present in less than 1%. The multiplicity of competing mechanisms and energetically similar structural types in organometallic chemistry has often been blamed for the poor state of mechanistic understanding in this field. One of the main reasons for the lack of quantitative structure-reactivity correlations in transition metal chemistry that would go beyond the qualitative achievements in this field (e.g. the isolobal analogy) is the paucity of quantitative thermochemical data for metal–ligand bond energies and elemental reaction steps for real-world organometallics. Although the binding of simple ligands, e.g. hydride, alkyl, CO, etc., in homoleptic complexes has been approached previously, reliable data for even marginally more complicated complexes is rare [48]. With the powerful physical techniques at hand, we are now in a position to address this task. A very useful method by which ion–ligand dissociation energies or ion fragmentation energies can be determined depends on threshold measurements for collision-induced dissociation. The CID threshold method utilizing tandem mass spectrometry has experienced significant growth and is currently used for quantitative measurements by several groups [49]. This methodology has been pioneered and continuously refined over the past 15 years by Armentrout and co-workers [4,50]. In principal, reduction of the experimentally observed threshold to meaningful chemical information requires two determinations: the structure of the initial ions needs to be determined, and the binding energy needs to be extracted from the experimental threshold. The measured intensities of the reactant and product ions are converted to a total cross section; the energy thresholds E_0 are then obtained by fitting the product ion energy profiles with the CRUNCH program developed by Armentrout and co-workers [49,51,52]. The fitting procedure is based on

$$\sigma = \sigma_0 \sum_i g_i (E + E_i + E_{\mathrm{rot}} - E_0)^n / E$$

where σ is the cross section, which is proportional to the observed product ion intensity at single collision conditions, E is the kinetic energy in the center-of-mass frame, E_I is the internal vibrational energy of the precursor ion whose relative abundance at a given temperature is g_i, where $\sum_i g_i = 1$, and E_0 is the threshold energy, corresponding to the energy required for the dissociation reaction at 0 K. The fitting procedure treats n and E_0 as variable parameters which are determined through the best fit. The vibrational energies E_i are calculated from the frequencies of the normal vibrations of the precursor ion. The frequencies are generally obtained from quantum chemical calculations. An important feature underlying the above equation is the assumption that due to the relatively long residence time of the excited ions in O2, dissociation at the threshold involves the process where the internal energy of the products is close to 0 K, i.e. essentially all the internal energy of the precursor ion is used up in the dissociation at the observed threshold.

3.2. Model studies

As a control to check that we could correctly measure CID thresholds with our experimental setup, we first reproduced experiments by Kebarle and co-workers [53] and Armentrout and co-workers [51] for the reaction $[(H_2O)_n \cdot (H_3O)]^+ \rightarrow [(H_2O)_{n-1} \cdot (H_3O)]^+ + H_2O$. The generation of protonated water clusters is particularly simple by electrospray of a 10^{-4} M aqueous HCl solution (Fig. 7, top). Thresholds were measured at four different, decreasing

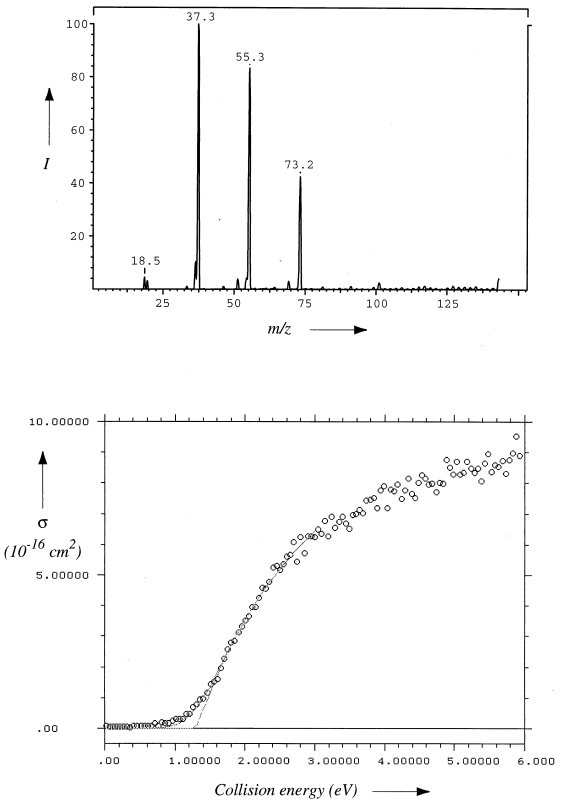

Fig. 7. (Top) Electrospray mass spectrum of a 10^{-4} M solution of HCl in H_2O under mild declustering conditions, showing the presence of different clusters $[(H_3O)(H_2O)_n]^+$, the clusters with $n = 1$, 2, and 3 being most prominent. (Bottom) CID threshold curve (collision gas Ar), showing the dependence of the dissociation cross section against collision energy, and fit to Armentrout's threshold function.

pressures and extrapolated to zero pressure in order to eliminate the contribution of multiple collisions to the foot of the threshold curve. The second parameter of crucial importance for precise CID threshold determinations is the internal energy distribution of the ion beam. Preferably, this should correspond to a Maxwell-Boltzmann distribution at a specific temperature. We have found that ~10 mTorr of Ar in the first octopole are sufficient for thermalization of ions produced by the electrospray source to the 70 °C manifold temperature. The threshold for $n = 1$, measured in daughter-ion mode, was extracted from our data with Armentrout's CRUNCH program, yielding a value of 1.29 eV (see Fig. 7, bottom) [30], in excellent agreement with the published data. For a second control experiment, we were looking for an organometallic ligand bond dissociation energy we could reproduce with our electrospray setup. We measured the threshold for the reaction $[Mn(CO)_6]^+ \rightarrow [Mn(CO)_5]^+ + CO$ in RFD mode as described above. A meaningful reaction enthalpy can be extracted from the threshold only when the initial kinetic energy distribution of the ions is narrow. With heavier ions, a narrow kinetic energy distribution is achievable when the first quadrupole is operated in RFD mode. The distribution in RFD mode is <0.6 eV FWHM in laboratory frame, corresponding to <0.1 eV in the center-of-mass frame and, furthermore, nearly Gaussian (argon or xenon as collision gas). Fitting the curve to Armentrout's threshold function yielded a value of 1.48 eV [54], also in good agreement with literature data [4]. When going to the reaction $[CpIr(PMe_3)(CH_3)]^+ \rightarrow [CpIr(\eta^2\text{-}CH_2PMe_2)]^+ + CH_4$, another factor comes into play which has to be taken into account. So far, the fits of the experimental profiles were based on the assumption that the energized reactant ions, whose total energy is equal or larger than E_0, will decompose within the residence time t of the ion in O2 before entering the mass analyzer Q2. For our experimental setup, complete dissociation within the residence time can be expected only for small polyatomic ions. Ions with many internal degrees of freedom will attain the required dissociation rate only at internal energies which are somewhat higher than E_0. This "kinetic shift" will lead to E_0 values that are too high. This effect becomes larger as the number of normal modes increases, making it non-negligible for the complexes described here. The kinetic shift can be corrected by including in the fitting procedure only the fraction of the precursor ions, which react during the residence time. This fraction can be evaluated with the Rice-Ramsperger-Kassel-Marcus (RRKM) formalism [55]. The quantitative CID threshold for the reaction $[CpIr(PMe_3)(CH_3)]^+ \rightarrow [CpIr(\eta^2\text{-}CH_2PMe_2)]^+ + CH_4$ and the kinetic energy distribution of the ion beam are shown in Fig. 8. The data were deconvoluted using Armentrout's CRUNCH program with the internal energy of the ions set by the 70 °C manifold temperature to which they were thermalized.

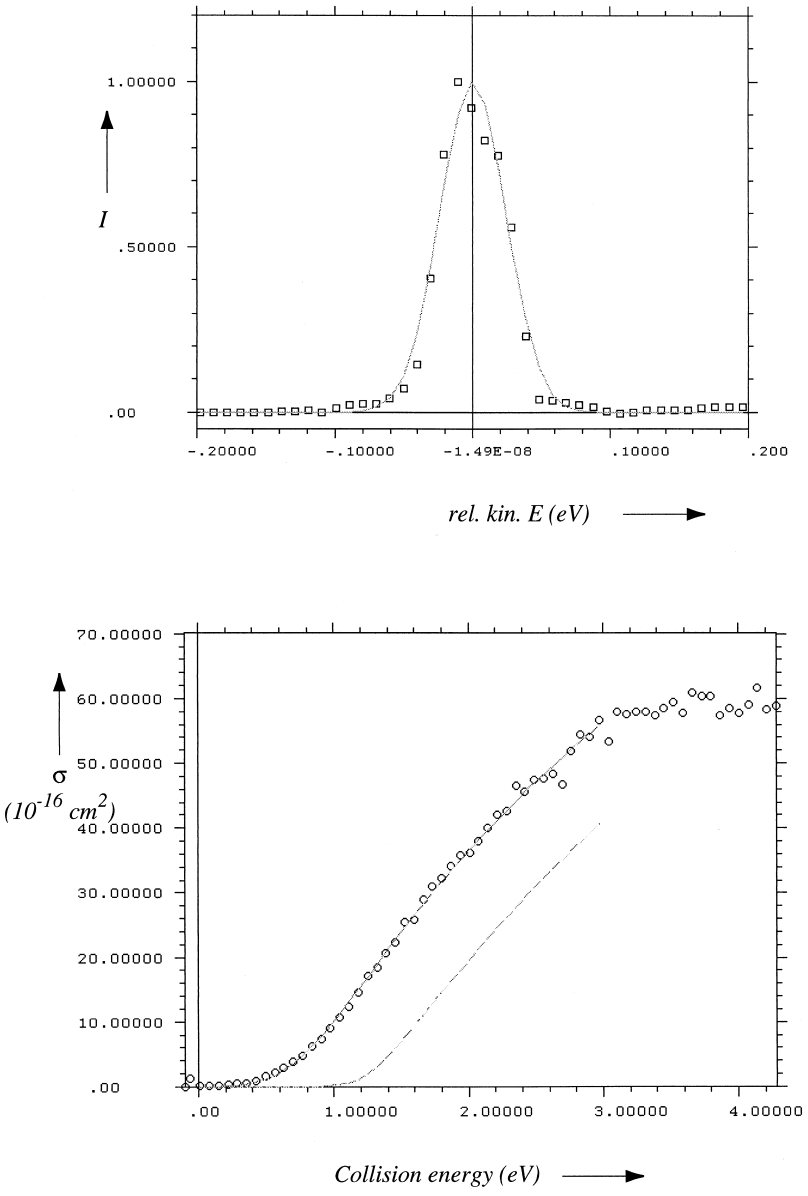

Fig. 8. (Top) Kinetic energy profile of $[CpIr(PMe_3)(CH_3)]^+$, measured in RFD mode. (Bottom) CID threshold curve (collision gas Ar).

Following the arguments by Armentrout and Squires [56,57], the values for transition-state frequencies can be assumed as follows. For an endothermic dissociation of gas-phase ions, a loose transition state can be assumed. Accordingly, the product frequencies can be used where available. For the five normal modes that correspond, at the asymptotic limit of dissociation, to relative rotations and translations of the departing fragments, further estimates have to be made. Numerical estimates for these five frequencies were taken from computations of analogous oxidative addition, reductive elimination, and σ-bond metathesis transition states. The deconvoluted threshold, with the methyl groups, the phosphine as a whole, and the

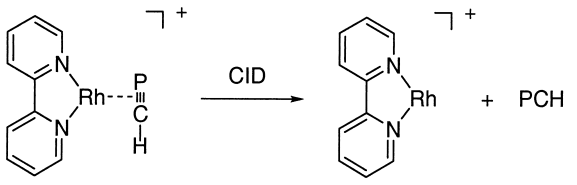

Scheme 9. Fragmentation of $[(bipy)Rh(P{\equiv}CH)]^+$ upon CID.

Cp ligand treated as internal rotors, yields a value of E_0 = 0.59 eV (13.6 kcal/mol).

In another application of the ES tandem-MS methodology for obtaining quantitative thermochemical data, the ligand binding energy in $[(bpy)Rh(P{\equiv}CH)]^+$ was recently determined (Scheme 9) [58]. The phosphaethyne complex was prepared in the gas phase by sequential loss of methane from the precursor ion $[(bpy)Rh(PMe_3)_2(H)_2]^+$ by collisional activation. Thermalization was achieved by ~10 mTorr N_2 in the first octopole. For the quantitative threshold measurement, the first quadrupole was operated in RFD mode as a high-pass filter, thereby rendering a narrow kinetic energy distribution of 0.4–0.5 eV FWHM (lab frame, xenon as collision gas). For the RRKM correction, calculations were performed at the B3LYP/LANL2DZ level. The side-on complex is favored over the end-on coordination by 25 kcal/mol at this level of theory. The five remaining transition-state frequencies for the kinetic-shift correction were obtained by taking the appropriate normal modes in the starting ion and reducing the frequencies by a factor of 2. Using these values, the threshold was fitted to yield $E_0 = 2.02 \pm 0.15$ eV.

As has now been demonstrated convincingly [30,58,59], the CID threshold methodology can be applied to molecules with relatively many degrees of freedom, yielding experimental thermochemical data of high quality. It is well known that enthalpies for transition-metal reactions and metal–ligand binding are notoriously difficult to calculate. In contrast to "simple" organic reactions, a systematic approach to the improvement of calculated reaction energies is not feasible for transition-metal compounds with full ligand spheres. Because of the restrictions of post-HF calculations on the system size, semi-empirical and hybrid ab initio/semi-empirical methods like DFT are clearly the methods of choice in this field. Unfortunately, there are severe restrictions on the possibility of a thorough parametrization of semi-empirical methods due to the lack of reliable thermochemical data for transition-metal binding. Thermochemical parameters derived from collision-induced dissociation threshold measurements could open the door to a pool of gas-phase data, which can directly be used for such parametrizations. Of course, since the deconvolution of the CID threshold measurement itself requires some kind of quantum chemical calculations for geometries and frequencies, one might conclude that such a procedure represents circular logic. However, previous experience suggests that geometries and frequencies are usually well modeled by DFT methods, yet the accuracy of these methods for the prediction of energy differences in transition metal complexes can be quite poor. The general success of DFT methods in predicting equilibrium geometries indicated that the local features of a potential surface in the immediate vicinity of a minimum are well treated. This means that a deconvolution scheme based on these frequencies should be sound. The relative energies of two separate minima, however, may not be equally well described. In this light, the use of the more reliable aspects of a computation to deconvolute experimental data that pertain to the less reliable aspects of that same computation is legitimate. Measurements of this kind should serve as benchmarks for the evaluation of the level of theory needed to obtain accurate thermochemistry for transition-metal complexes.

4. Conclusions

Electrospray mass spectrometry has unique advantages for the study of organometallic reaction mechanisms when compared to established condensed-phase methods.

Extremely reactive species can be stabilized or generated in the gas phase, as shown for $[Cp^*Ir(PMe_3)(CH_3)]^+$ and $[Cp_2ZrCH_3]^+$.

ESMS can be used as an analytical tool for

transient solution-phase species, if their concentration is high enough for detection, as shown in the case of $[(salen)Mn^{V}{=}O]^{+}$.

Single reaction steps can be studied by ion–molecule reactions in the collision cell.

Thermochemical parameters can be determined by using the CID threshold methodology, as shown for the endothermic reaction $[CpIr(PMe_3)(CH_3)]^{+} \rightarrow [CpIr(\eta^2\text{-}CH_2PMe_2)]^{+} + CH_4$.

Regions of relatively high pressure can be introduced for thermalization and reactions, which can serve to bridge the gap between solution-phase and gas-phase conditions, as demonstrated for the reaction of $[Cp_2ZrCH_3]^{+}$ with olefins.

ESMS allows real-world organometallics to be studied by ion–molecule techniques, thus immensely enhancing the possibilities of studying reaction mechanisms relevant for large-scale catalytic processes.

We have so far applied electrospray tandem mass spectrometry to the study of some of the most important transition metal-mediated reactions, namely C–H activation, oxygen transfer, and olefin polymerization. While the new method has already brought a wealth of new insights into organometallic chemistry, a vast field of possible applications remains unexplored, and the full potential of ESMS in reactivity studies has still to be exploited.

Acknowledgements

The author is very much indebted to Prof. Peter Armentrout for making the CRUNCH program available to us and for his kind support in the use of this program.

References

[1] B.S. Freiser, Organometallic Ion Chemistry, Kluwer, Dordrecht, 1996.
[2] D. Schröder, H. Schwarz, J. Phys. Chem. A 103 (1999) 7385.
[3] D. Schröder, H. Schwarz, Angew. Chem. Int. Ed. Engl. 34 (1995) 1973.
[4] P.B. Armentrout, Acc. Chem. Res. 28 (1995) 430.
[5] M.T. Rodgers, P.B. Armentrout, Mass Spectrom. Rev. 19 (2000) 215.
[6] Recent, representative work: I. Kretzschmar, D. Schröder, H. Schwarz, C. Rue, P.B. Armentrout, J. Phys. Chem. A 104 (2000) 5046; M. Brönstrup, C. Trage, D. Schröder, H. Schwarz, J. Am. Chem. Soc. 122 (2000) 699; M. Diefenbach, M. Brönstrup, M. Aschi, D. Schröder, H. Schwarz, ibid. 121 (1999) 10614; M. Brönstrup, D. Schröder, H. Schwarz, Organometallics 18 (1999) 1939; G. Hornung, S. Bärsch, D.Schröder, H. Schwarz, ibid. 17 (1998) 2271; M. Aschi, M. Brönstrup, M. Diefenbach, J.N. Harvey, D. Schröder, H. Schwarz, Angew. Chem. Int. Ed. Engl. 37 (1998) 829; A. Andersen, F. Muntean, D. Walter, C. Rue, P.B. Armentrout, J. Phys. Chem. A 104 (2000) 692; M.T. Rodgers, P.B. Armentrout, ibid. 103 (1999) 4955; M.R. Sievers, P.B. Armentrout, Inorg. Chem. 38 (1999) 397; P.A.M. van Koppen, M.T. Bowers, C.L. Haynes, P.B. Armentrout, J. Am. Chem. Soc. 120 (1998) 5704; D. Walter, P.B. Armentrout, ibid. 120 (1998) 3176; S.W. Lee, S.B. Chang, D. Kossakovski, H. Cox, J.L. Beauchamp, ibid. 121 (1999) 10152; K.C. Crellin, J.L. Beauchamp, W.A. Goddard, S. Geribaldi, M. Decouzon, Int. J. Mass Spectrom. 183 (1999) 121; K.C. Crellin, J.L. Beauchamp, S. Geribaldi, M. Decouzon, Organometallics 15 (1996) 5368; H.P. Chen, D.B. Jacobson, B.S. Freiser, J. Phys. Chem. A 103 (1999) 10884; Q. Chen, C. Sioma, S.Z. Kan, B.S. Freiser, Int. J. Mass Spectrom. 180 (1998) 231; Q. Chen, B.S. Freiser, J. Phys. Chem. A 102 (1998) 3343.
[7] Electrospray Ionization Mass Spectrometry, R.B. Cole (Ed.), Wiley, New York, 1997.
[8] Biochemical and Biotechnological Applications of Electrospray Ionization Mass Spectrometry, A.P. Snyder (Ed.), ACS. Symp. Ser. 619 (1995).
[9] A good overview of applications of ESMS to the analysis of biomacromolecules can be found in: M. Przybylski, M.O. Glocker, Angew. Chem. Int. Ed. Engl. 35 (1996) 806.
[10] A.G. Bailey, Electrostatic Spraying of Liquids, Research Studies Press, Taunton, Somerset, UK, 1988.
[11] In contrast to Dole's "charge residual model" (CRM), a different mechanism for the last stage of free ion formation in the electrospray process, the so-called "ion evaporation model" (IEM), was proposed in J.V. Iribarne, B.A. Thomson, J. Chem. Phys. 64 (1976) 2287; B.A. Thomson, J.V. Iribarne, ibid. 71 (1979) 4451. For a discussion of the current view on the mechanism of ion formation in electrospray, see: J.B. Fenn, J. Rosell, T. Nohmi, S. Shen, F.J. Banks Jr., Electrospray Ion Formation: Desorption Versus Desertion, in [8], p.60; P. Kebarle, Y. Ho, On the Mechanism of Electrospray Mass Spectrometry, in [7], p.3.
[12] M. Dole, R.L. Hines, L.L. Mack, R.C. Mobley, L.D. Ferguson, M.B. Alice, Macromolecules 1 (1968) 96.
[13] M. Dole, L.L. Mack, R.L. Hines, R.C. Mobley, L.D. Ferguson, M.B. Alice, J. Chem. Phys. 49 (1968) 2240.
[14] L.L. Mack, P. Kralik, A. Rheude, M. Dole, J. Chem. Phys. 52 (1970) 4977.
[15] G.A. Clegg, M. Dole, Biopolymers 10 (1971) 821.
[16] A very personal account of the route to electrospray mass spectrometry was published by J. B. Fenn as a foreword to a recent monograph, see [7].
[17] M. Yamashita, J.B. Fenn, J. Phys. Chem. 88 (1984) 4451.
[18] M. Yamashita, J.B. Fenn, J. Phys. Chem. 88 (1984) 4671.
[19] C.M. Whitehouse, R.N. Dreyer, M. Yamashita, J.B. Fenn, Anal. Chem. 57 (1985) 675.

[20] J.B. Fenn, M. Mann, C.K. Meng, S.F. Wong, C.M. Whitehouse, Science 246 (1989) 64.
[21] V. Katta, S.K. Chowdhury, B.T. Chait, J. Am. Chem. Soc. 112 (1990) 5348.
[22] R. Colton, A. D'Agostino, J.C. Traeger, Mass Spectrom. Rev. 14 (1995) 79, and references cited therein.
[23] W. Henderson, B.K. Nicholson, L.J. McCaffrey, Polyhedron 17 (1998) 4291.
[24] (a) T.G. Spence, T.D. Burns, L.A. Posey, J. Phys. Chem. A 101 (1997) 139 (b) T.G. Spence, T.D. Burns, G.B. Guckenberger, L.A. Posey, ibid. 101 (1997) 1081; (c) T.G. Spence, B.T. Trotter, T.D. Burns, L.A. Posey, ibid. 102 (1998) 6101.
[25] B.A. Arndtsen, R.G. Bergman, T.A. Mobley, T.H. Petersen, Acc. Chem. Res. 28 (1995) 154.
[26] A.H. Janowicz, R.G. Bergman, J. Am. Chem. Soc. 104 (1982) 352; W.D. Jones, F.J. Feher, ibid. 106 (1984) 1650; J.K. Hoyano, A.D. McMaster, W.A.G. Graham, ibid. 105 (1983) 7190.
[27] P. Burger, R.G. Bergman, J. Am. Chem. Soc. 115 (1993) 10462; B.A. Arndtsen, R.G. Bergman, Science 270 (1995) 1970; J.E. Veltheer, P. Burger, R.G. Bergman, J. Am. Chem. Soc. 117 (1995) 12478.
[28] D.L. Strout, S. Zaric, S. Niu, M.B. Hall, J. Am. Chem. Soc. 118 (1996) 6068.
[29] C. Hinderling, D.A. Plattner, P. Chen, Angew. Chem. Int. Ed. Engl. 36 (1997) 243.
[30] C. Hinderling, D. Feichtinger, D.A. Plattner, P. Chen, J. Am. Chem. Soc. 119 (1997) 10793.
[31] H.F. Luecke, R.G. Bergman, J. Am. Chem. Soc. 119 (1997) 11538.
[32] (a) T.L. Siddall, N. Miyaura, J.C. Huffman, J.K. Kochi, J. Chem. Soc., Chem. Commun. (1983) 1185; (b) E.G. Samsel, K. Srinivasan, J.K. Kochi, J. Am. Chem. Soc. 107 (1985) 7606; (c) K. Srinivasan, J.K. Kochi, Inorg. Chem. 24 (1985) 4671; (d) K. Srinivasan, P. Michaud, J.K. Kochi, J. Am. Chem. Soc. 108 (1986) 2309; (e) K. Srinivasan, S. Perrier, J.K. Kochi, J. Mol. Cat. 36 (1986) 297.
[33] J.T. Groves, W.J. Kruper, J. Am. Chem. Soc. 101 (1979) 7613.
[34] W. Zhang, J.L. Loebach, S.R. Wilson, E.N. Jacobsen, J. Am. Chem. Soc. 112 (1990) 2801.
[35] R. Irie, K. Noda, Y. Ito, N. Matsumoto, T. Katsuki, Tetrahedron Lett. 31 (1990) 7345.
[36] D. Feichtinger, D.A. Plattner, Angew. Chem. Int. Ed. Engl. 36 (1997) 1718.
[37] D. Feichtinger, D.A. Plattner, J. Chem. Soc., Perkin Trans. 2 (2000) 1023.
[38] D.A. Plattner, D. Feichtinger, J. El-Bahraoui, O. Wiest, Int. J. Mass Spectrom. 195/196 (2000) 351.
[39] D. Feichtinger, D.A. Plattner, Chem. Eur. J., 7 (2001) 591.
[40] A similar method that translates kinetic branching ratios into thermochemical data in cases where the difference of entropy change between two different fragmentation pathways can be neglected was introduced by Cooks. The assumptions inherent in the "Cooks' kinetic method" are essentially the same as those required for linear free energy relationships, i.e. Hammett $\sigma\rho$ correlations. The kinetic method has been widely used for the determination of proton affinities and gas-phase basicities of many organic compounds, yielding values in excellent agreement with independent methods: R.G. Cooks, J.S. Patrick, T. Kotiaho, S.A. McLuckey, Mass Spectrom. Rev. 13 (1994) 287; R.G. Cooks, P.S.H. Wong, Acc. Chem. Res. 31 (1998) 379, and references cited therein.
[41] H.C. Brown, Y. Okamoto, J. Am. Chem. Soc. 80 (1958) 4979.
[42] Ziegler Catalysts, G. Fink, R. Mülhaupt, H.H. Brintzinger (Eds.), Springer, New York, 1995.
[43] R.F. Jordan, W.E. Dasher, S.F. Echols, J. Am. Chem. Soc. 108 (1986) 1718; R.F. Jordan, C.S. Bajgur, R. Willett, B. Scott, ibid. 108 (1986) 7410.
[44] H.H. Brintzinger, D. Fischer, R. Mülhaupt, B. Rieger, R. Waymouth, Angew. Chem. Int. Ed. Engl. 34 (1995) 1143.
[45] C.S. Christ, J.R. Eyler, D.E. Richardson, J. Am. Chem. Soc. 110 (1988) 4038; 112 (1990) 596; D.E. Richardson, N.G. Alameddin, M.F. Ryan, T. Hayes, J.R. Eyler, A.R. Siedle, ibid. 118 (1996) 11244.
[46] D. Feichtinger, D.A. Plattner, P. Chen, J. Am. Chem. Soc. 120 (1998) 7125.
[47] J.C.W. Chien, B.P. Wang, J. Polym. Sci., Part A 28 (1990) 15.
[48] J.A. Martinho Simões, J.L. Beauchamp, Chem. Rev. 90 (1990) 629.
[49] P.B Armentrout, Thermochemical Measurements by Guided Ion Beam Mass Spectrometry, in N. Adams, L.M. Babcock (Eds.), Advances in Gas Phase Ion Chemistry, JAI Press, Greenwich, CT, 1992, Vol. 1, p 83, and references cited therein.
[50] K.M. Ervin, P.B. Armentrout, J. Chem. Phys. 83 (1985) 166; S.K. Loh, D.A. Hales, L. Lian, P.B. Armentrout, ibid. 90 (1989) 5466; R.H. Schultz, P.B. Armentrout, Int. J. Mass Spectrom. Ion Processes 107 (1991) 29; N.F. Dalleska, K. Honma, L.S. Sunderlin, P.B. Armentrout, J. Am. Chem. Soc. 116 (1994) 3519; M.T. Rodgers, K.M. Ervin, P.B. Armentrout, J. Chem. Phys. 106 (1997) 4499.
[51] N.F. Dalleska, K. Honma, P.B. Armentrout, J. Am. Chem. Soc. 115 (1993) 12125.
[52] P. Armentrout, pivate communication.
[53] S.G. Anderson, A.T. Blades, J. Klassen, P. Kebarle, Int. J. Mass Spectrom. Ion Processes 141 (1995) 217.
[54] C. Hinderling, D.A. Plattner, unpublished results.
[55] K.A. Holbrook, M.J. Pilling, S.H. Robertson, Unimolecular Reactions, Wiley, Chichester, 1996.
[56] R.H. Schultz, K.C. Crellin, P.B. Armentrout, J. Am. Chem. Soc. 113 (1991) 8590; F.A. Khan, D.E. Clemmer, R.H. Schultz, P.B. Armentrout, J. Phys. Chem. 97 (1993) 7978.
[57] L.S. Sunderlin, D. Wang, R.R. Squires, J. Am. Chem. Soc. 115 (1993) 12060.
[58] Y.-M. Kim, P. Chen, Int. J. Mass Spectrom. 202 (2000) 1.
[59] J.S. Klassen, S.G. Anderson, A.T. Blades, P. Kebarle, J. Phys. Chem. 100 (1996) 14218.